Magnetic Shielding Free Rubidium Magnetometer

A thesis submitted in partial fulfillment of the requirements for the degree of Bachelor of Science degree in Physics from the College of William and Mary

by

Zach Thomas

Advisor: Irina Novikova

Senior Research Coordinator: Gina L. Hoatson

Date: May 8, 2017

TABLE OF CONTENTS

1. Abstract

The magnetometer that I have constructed is able to measure the magnetic field even in the Earth's magnetic field while in a magnetic shielding free setup and is capable of measuring the magnetic field vectors. To measure the magnetic fields in the laboratory setup we constructed a heating element in order to warm the Rb cell without creating a magnetic field. Then we used this setup to measure the EIT and used these measurements in order to calculate the magnetic Field vectors. We calculated the magnetic field to be approximately .651G and the direction to be approximately at the 0 degree position, which was very close to the background measurements taken. Then we sought out to optimize the EIT measurements to get much clearer signals and also to eliminate noise.

2. Introduction

2.1 Magnetometers

In the past the usage of magnetometers, such as Hall probes and fluxgate, were used to aid in the fields of geo-sensing and navigation. Magnetometers have been used for a variety of purposes ranging from medical facilities, to digging for oil. However in the 1970's magnetometers began to be redesigned in order to use atomic and quantum mechanical principles to measure magnetic fields. This in turn led to an increase in the sensitivity of magnetometers. These magnetometers can even measure into the 10-15 Tesla level.[1] These advances made the atomic magnetometers indispensable from modern day material testing.[2] The EIT (Electromagnetically Induced Transparency) magnetometer used in this experiment, is at least 5 orders of magnitude more sensitive than the fluxgate magnetometers. These magnetometers operate at zero background magnetic fields. However, the Earth has .5mT field so they have to enclose these magnetometers in magnetic shield casings. This then limits the magnetometer's measurements in Earth's magnetic field. An EIT is the effect, which is created when a 3 level quantum mechanical system is properly aligned between 2 laser fields and becomes transparent. We will be using this EIT field in order to allow us to measure the magnetic field using the spectroscopy of Rubidium atoms.

2.2 Electromagnetically Induced Transparency (EIT)

As the name suggests an Electromagnetically Induced Transparency or EIT refers to when an atom or a group of atoms becomes transparent when electromagnetic fields are applied. This occurs when two lasers are tuned from two different ground states to the same excited state, as shown in Figure 1. This in turn causes the medium to become transparent. An image for this three level

system is depicted below.

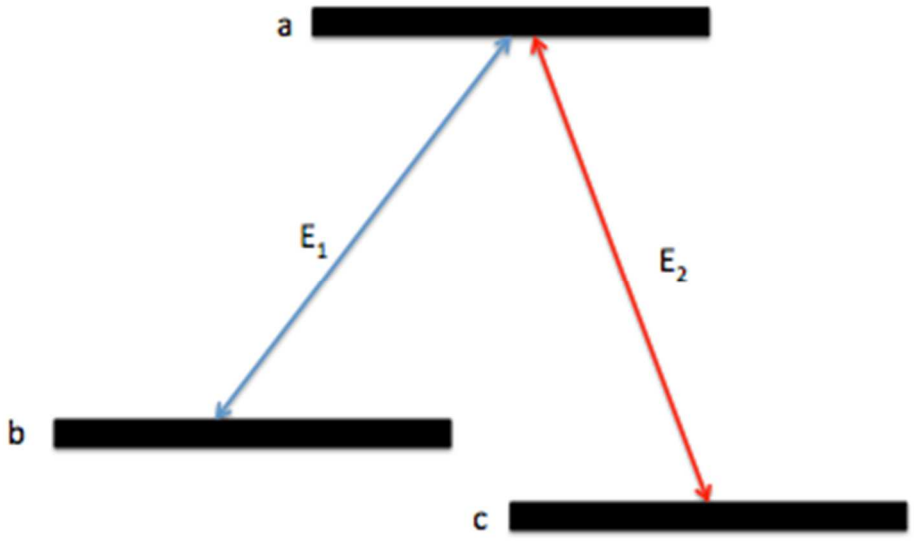

Figure 1: A three level system where b and c are ground states, a is the excited state and the two optical fields are E1 and E2.

The EIT can be illustrated through a quantum mechanics perspective using time dependent perturbation theory [3]. In this equation c_a, c_b and c_c are the time dependent population densities of the states a, b and c recorded in Figure 1. Which can then be applied to the equation

$$\Psi = c_a(t)\psi_a e^{-iEat/\hbar} + c_b(t)\psi_b e^{-iEbt/\hbar} + c_c(t)\psi_c e^{-iEct/\hbar}$$

Using this wavefunction in the time dependent Schrodinger equation we get the matrix equation.

$$\begin{pmatrix} H'_{aa} & H'_{ab} & H'_{ac} \\ H'_{ba} & H'_{bb} & H'_{bc} \\ H'_{ca} & H'_{cb} & H'_{cc} \end{pmatrix} \begin{pmatrix} c_a e^{-iEat/\hbar} \\ c_b e^{-iEbt/\hbar} \\ c_c e^{-iEct/\hbar} \end{pmatrix} = ih\,\partial/\,\partial t \begin{pmatrix} c_a e^{-iEat/\hbar} \\ c_b e^{-iEbt/\hbar} \\ c_c e^{-iEct/\hbar} \end{pmatrix}$$

Where the matrix $\hat{H}$ represents the Hamiltonian of the system. However in the simplified case as shown in Figure 1 E_1 only interacts with a and b states while E_2 only acts with the a and c states. Therefore we can write the matrix as written below where Ω1 and Ω2 are the Rabi frequencies of oscillations. In this equation Ω1 refers to the transition from a to c and Ω2 refers to the transition a-b.

$$i\frac{\partial}{\partial t}c_a = \Omega_1 c_b e^{i(w_1 - w_{ab})t} + \Omega_2 c_c e^{i(w_2 - w_{ac})t}$$

$$i\frac{\partial}{\partial t}c_b = \Omega_1 c_a e^{i(w_2 - w_{ab})t}$$

$$i\frac{\partial}{\partial t}c_c = \Omega_1 c_a e^{i(w_1 - w_{ac})t}$$

EIT will only occur when $\partial/\partial t\, c_a = 0$ so this will only occur in the equation

$$\Omega_1 c_b = -\Omega_2 c_c e^{it[(\omega_2 - \omega_{ac}) - (\omega_1 - \omega_{ab})]}$$

This equation will then provide the fact that ω_1-ω_2 must be equal to ω_{bc}, which is the difference in energy levels between levels b and c. This is called two-photon resonance and through this no atoms in b and c levels will transition into the a level and thus we can successfully achieve EIT. Then using this information we can determine where the dark state occurs.[4] The dark state is the state in which the incident laser does not interact. Its counter part is the bright state in which the incident laser does interact. It is thanks to these dark and bright states that we are able to make the medium transparent. The process works so that if an atom enters an excited state it will decay into a dark or bright state. If it enters the dark state it will remains trapped in the dark state, and stops interacting with light. However, if it enters a bright state then it will go through the process again. As such eventually everything will enter the dark state, allowing the light to travel through the atomic medium without absorption.

2.3 Rubidium in Magnetic Fields

There are only two ways in which a rubidium atom can respond to a magnetic field, which is the Zeeman effect and the quantization of the magnetic dipole moments. The Zeeman effect in our experiment is responsible for the source of the ground state energy levels being sensitive to the magnetic fields. This in turn can be used to measure the magnetic field for rubidium 87, which is equivalent to the formula. In this formula u_B is the Bohr magneton, g is the gyromagnetic ratio, m is the azimuthal angular momentum quantum number and Δf is the change in frequency between the transmission peaks.

$$\Delta f = m \cdot g \cdot \mu_B \cdot B \qquad (1)$$

In our experiment uB*g=(.7MHz/G) for the rubidium 87. The magnetic dipole moment of the atom is also in the direction of the magnetic field. We can then use the magnetic field to specify a z-direction for the atoms. If both of these effects were measured then we are able to measure the Zeeman splitting, and direction of the magnetic field due to the difference in interaction strength for light of different polarization with the projection direction m. To measure these values we use the EIT magnetometer.

3. Experimental Setup

3.1 Assembly Magnetic Field Casing

This experiment's first goal was to create a magnetic shielding-free rubidium magnetometer and to do so I had to assemble all of the necessary components. The project originally consisted of a holder designed to hold the rubidium cell and had holes drilled through it to allow for tubing to pass through.

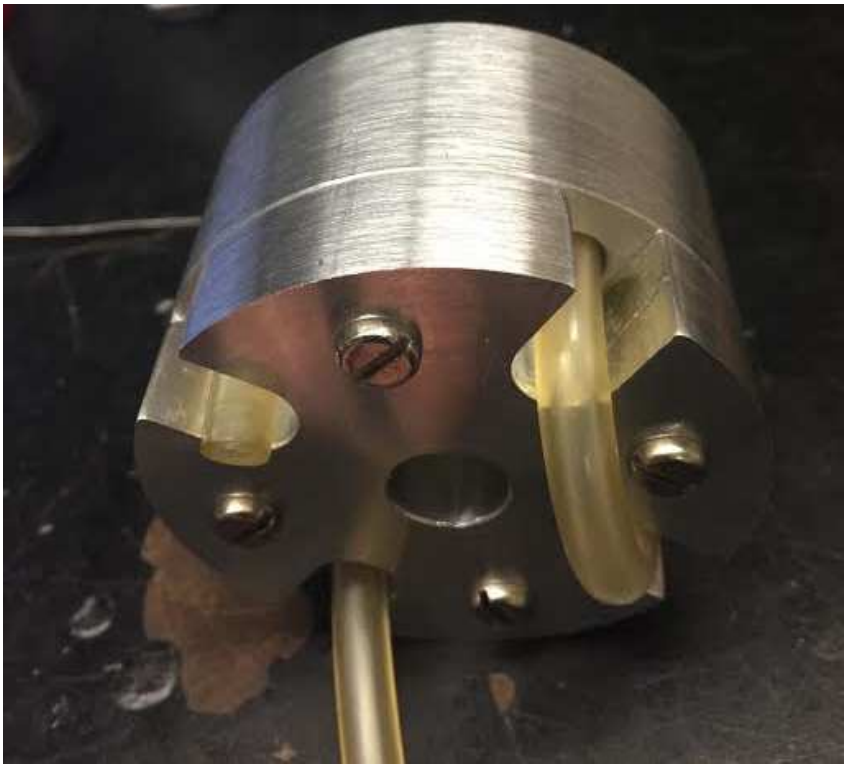

Figure 2: The rubidium cell holder

I had to devise a system to heat this apparatus and ensure that a laser could pass through the rubidium cell uninterrupted. To do so I first needed a t-connector to branch this new air pathway from the existing air pathway. Then I needed an airflow control valve in order control the airflow speed. In order for the rubidium cell to be heated most efficiently only a certain amount of air could pass through at a time. After the appropriate airflow was established I needed a heater and a pipe to tubing connector in order to attach the heater to the tubing. To ensure safety and improve the thermo-isolation I also attached a fiber glass cover around the heater and wrapped the heater with a high temperature taping

to ensure that there would be no accidents with the heater burning others or interfering in the experiment in unexpected ways. Then we had to get tubing that was able to handle above 100^0C. However, the tubing also had to be very flexible as we discovered that any rigid tubing would not allow enough airflow to pass through the apparatus. Another limitation of the tubing was that the airflow pressure through the tubing could not be less than 15 psi for the apparatus to heat in a reasonable manner and for the heater to not be overheating itself. In order to avoid losing too much energy, the tubing was also firmly wrapped in a fiberglass cover and covered with a heat resistant tape. Lastly, for safety's sake a temperature controller was attached to the apparatus in order to ensure that the rubidium cell and tubing would not be overheated and either malfunction or deform. The experimental parameters for this setup were set to ensure that no deformations would occur in the apparatus. As such the temperature could range from 25^0C – 100^0C. To ensure the proper airflow regulation there was no more than 15psi inside the tubing. However, for the most part of these experiments the psi was approximately 12psi. Lastly, to ensure the proper voltage was sent through the temperature controller we used a variac. This variac Voltage was set to be 40V.

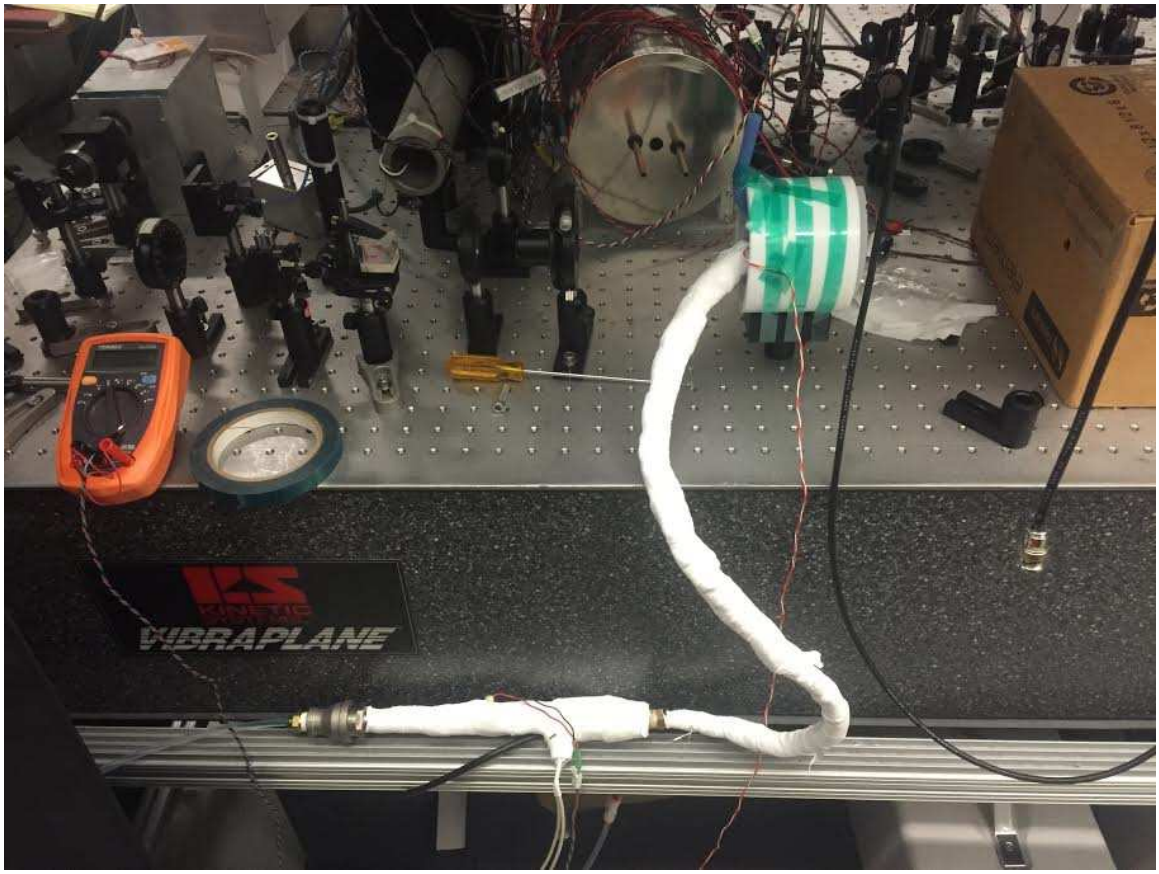

Figure 3: The heating apparatus.

The next step for this part of the experimental setup consisted of aligning the optical components to allow a beam to pass through the rubidium cell. To do this a mirror was used to change the optical pathway of the laser. The optical alignment consisted of a beam splitter, a wave plate and a polarizer. This setup of the optical pathway was designed to ensure that only a polarized light is able to go through the rubidium cell and is recorded in Figure 4. In this image a laser shines through the polarizing beam splitter then through the wave plate. Then it goes through the polarizer and then passes through the Rubidium cell holder as detailed below. Lastly it goes into a photodiode detector, which feeds the information into a computer, which displays the recorded waveform. Then it goes through a 6.835 GHz Synthesizer. Then the DAVLL's (Dichroic Atomic Vapor Laser Lock) function is to stabilize the laser's frequency to be approximately 795nm.

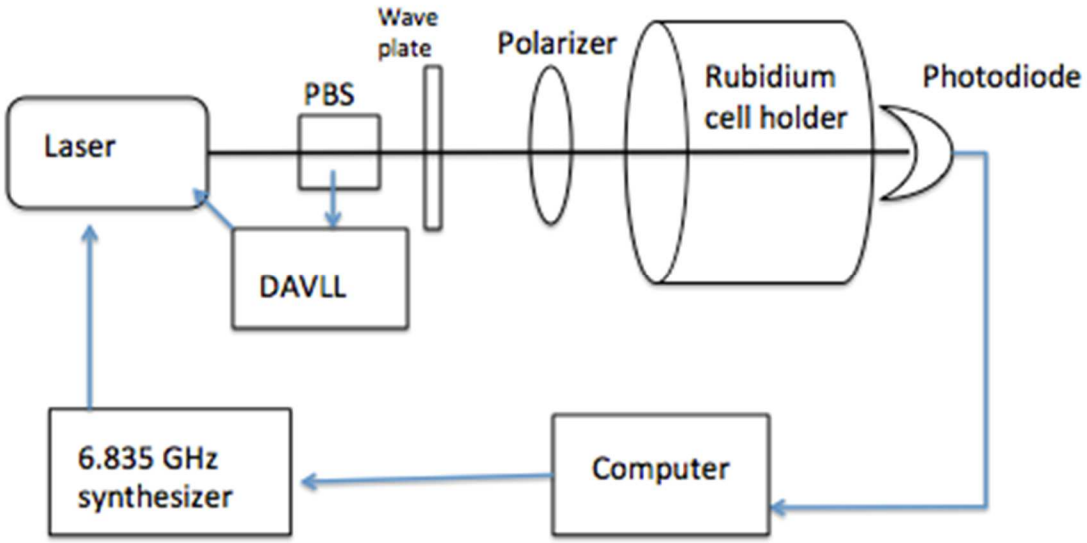

Figure 4: Experimental Setup

In order for an EIT signal to occur it requires 2 laser fields coupled into a 3-level system. To scan resonances the laser field must be precisely controlled and the phases of the laser fields must match. To do this we used a single frequency laser that is current modulated at 6.835GHz. This allows us to scan the relative frequency of two EIT fields and observe changes in transmission. Using this modulation and the DAVLL we would then tune the frequency to the F=1 to F'=1 transition as well as the F=2 to F'=1 transition. The laser that we use in this experiment is known as a VCSEL Laser and is the laser commonly used in atomic clocks and magnetometer experiments due to its high tunability.

3.2 Background Magnetic Field

In order for the magnetometer to work correctly we needed to minimize the amount of inhomogeneous background magnetic fields. For our experiment we tried to eliminate all the possible sources for the magnetic fields. We removed all the magnetic mounts on the laser equipment within a 30 cm area, as anywhere outside of a 20 cm area did not have an effect upon the magnetic field. We also moved the apparatus farther from the edge of the table, as there was a higher value background magnetic field. We also had to remove the previously used

magnetic shielding from the table as we determined that they had a huge magnetic field.

I created a map of the magnetic field in a 3-inch cube around where the rubidium cell would be located. To do this we used a commercial fluxgate magnetometer, and measured the magnetic field in all three directions. A general image of the setup of this can be found in Figure 5.

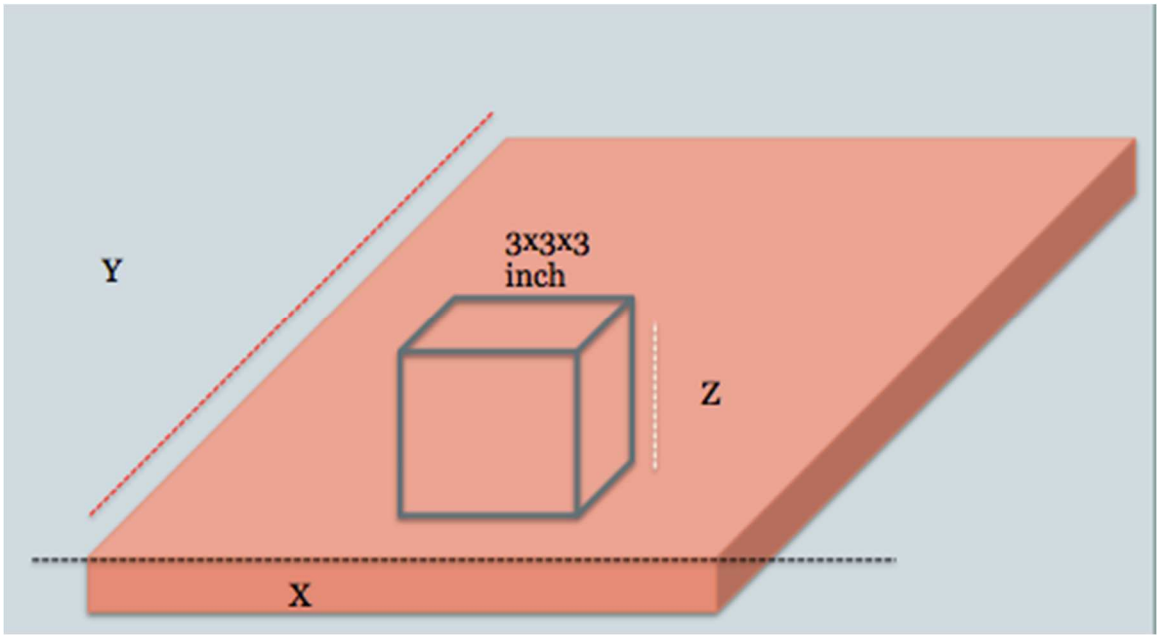

Figure 5: This illustration is the orientation of the map for the magnetic field measurements.

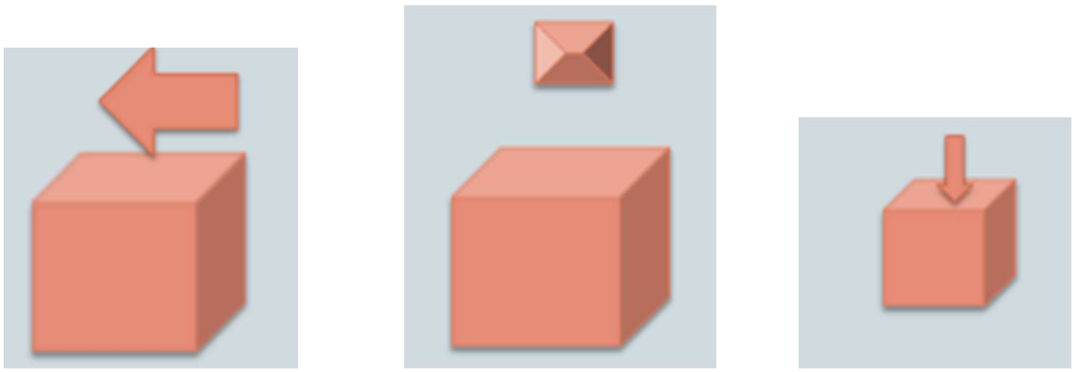

X Directional orientation Y Directional Orientation Z Directional Orientation

Figure 6: These illustrations shows the direction associated with each vector component of the magnetic field.

We determined the magnetic field in the y direction to be relatively stable regardless of the height. This is illustrated in Figure 7. As there was only a .02 G difference in the Gauss when the height was changed.

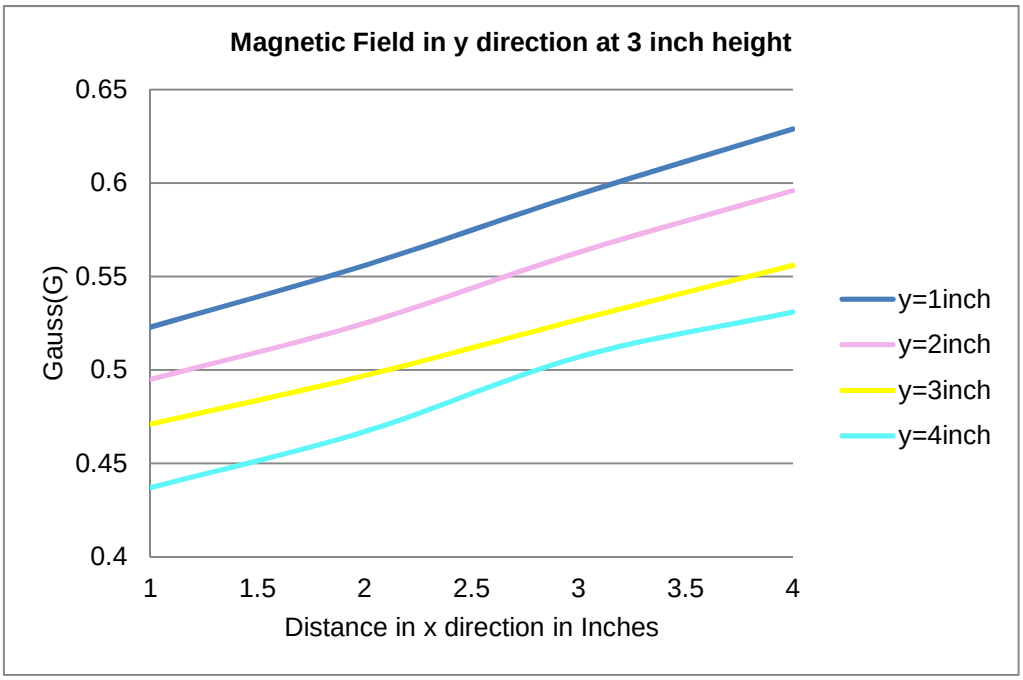

Figure 7: A graph of the magnetic field at the 4-inch height with the magnetic field in the y direction

The magnetic field in the x direction was also fairly consistent. There was a difference in the field was more dramatic than the y direction however it was only a difference of .03 G. This is displayed in Figure 8.

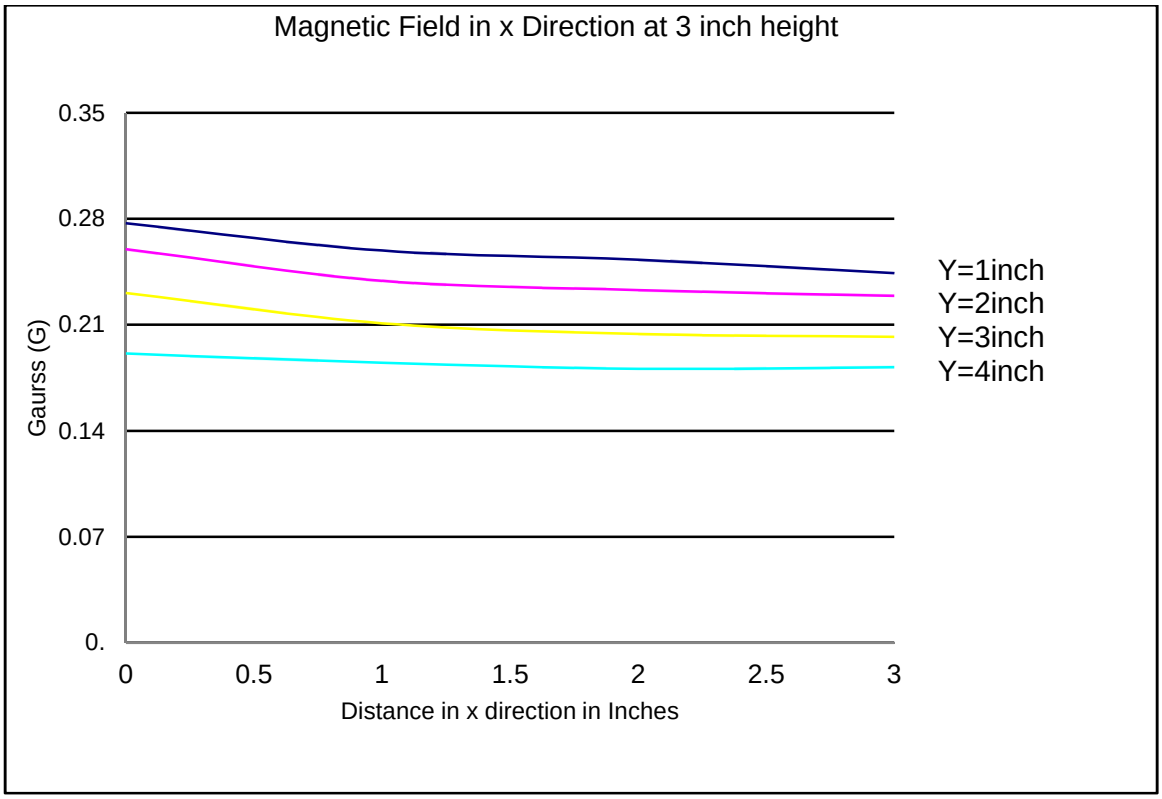

Figure 8: A graph of the magnetic field at the 4-inch height with the magnetic field in the x direction

The Magnetic field in the z direction was not at all consistent. There was a difference in the field more dramatic than any other directions. The magnetic field in the z direction also had a bizarre appearance as below the 4-inch mark they are increasing and it isn't until the 4-inch height that the field becomes relatively stable. This z direction is the reasoning behind the height of 4-inches being chosen for the ideal height for the rubidium cell to be at. This is located in Figure 9.

Therefore we decided to mount the magnetometer at the three-inch height and 2 inches in the x direction and 2 inches in the y direction. At this point we had the most stable background magnetic field. The value of the magnetic field in the x direction was .233G, the value of the magnetic field in the y direction was .603 G and the value of the magnetic field in the z direction was .083 G.

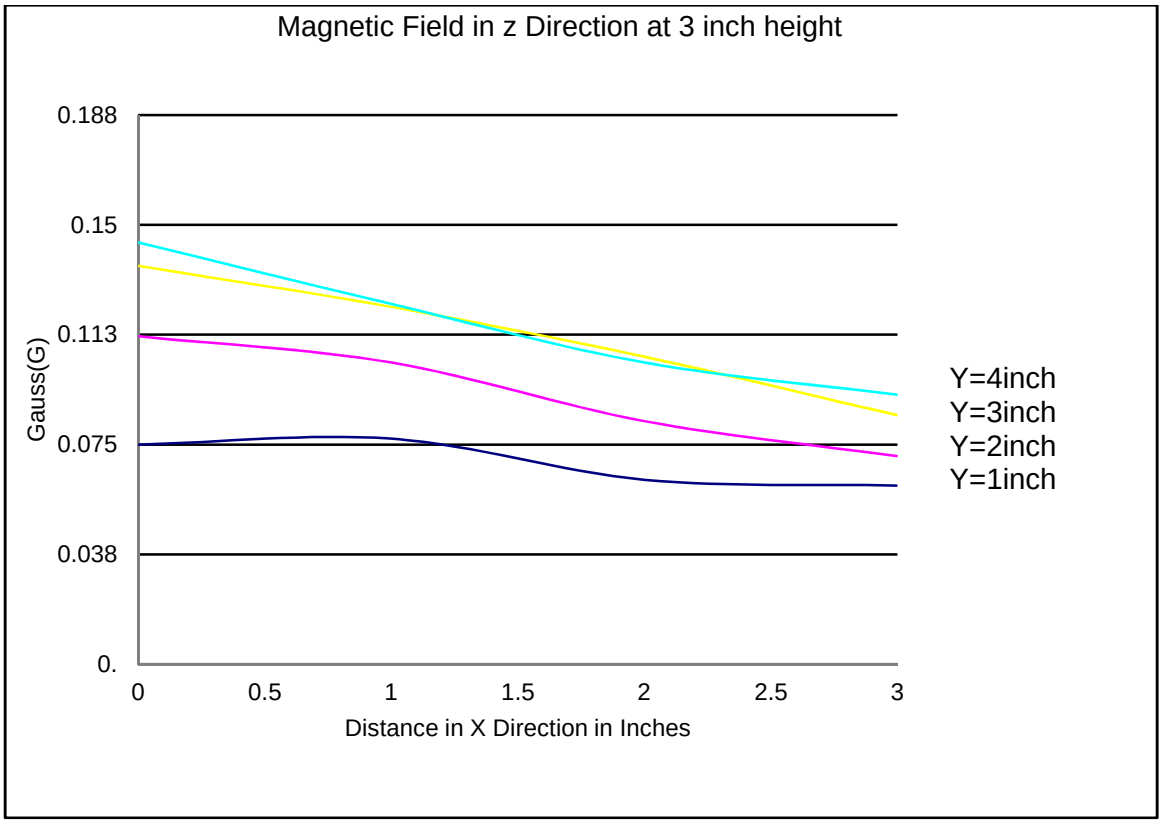

Figure 9: A graph of the magnetic field at the 4-inch height with the magnetic field in the z direction

4. Data Analysis

4.1 Rb Vapor Density Calibration

For our experiment we measured the atomic density of Rubidium in order to find out how many atoms of Rubidium are undergoing an atomic transition. We then used this number of atoms undergoing an atomic transition in order to determine the number of atoms that are currently in a vapor state and are interacting with the laser. We did this by shining a laser through the apparatus into a photodiode detector and observing the wave function produced. We then compared this information to the expected value using a Mathematica program and used this in order to determine how many atoms are currently undergoing this transition depending upon the temperature.

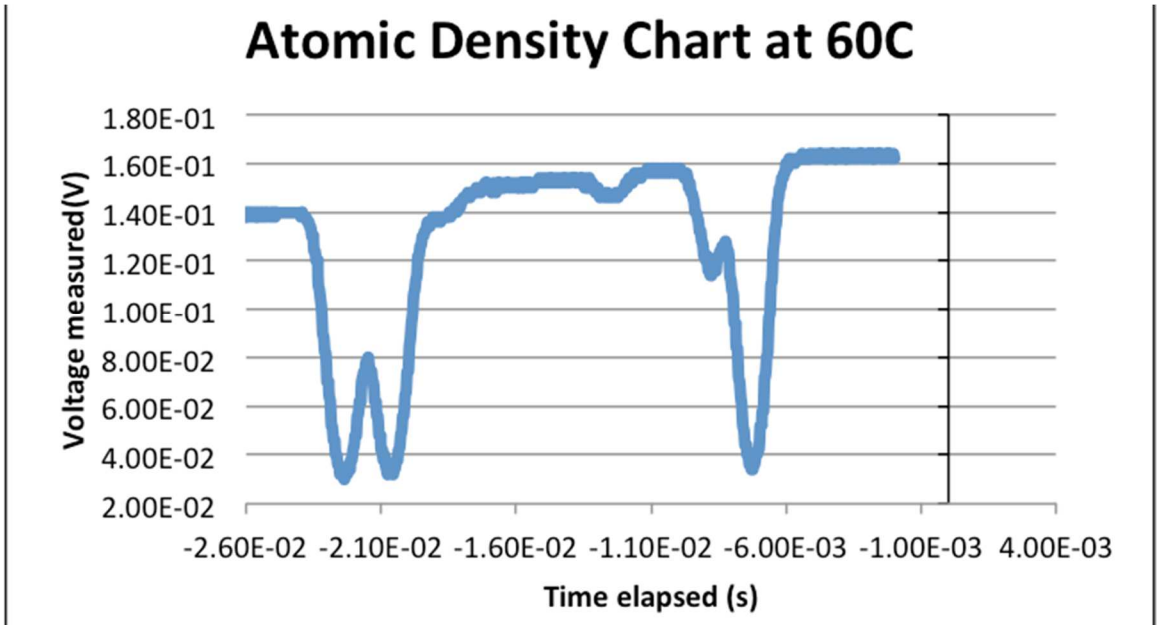

Figure 10: a graph of cell transmission Rubidium looks like at 60^{o}C.

We then conducted these trials from the temperature of 25^{o}C progressing to 100^{o}C. Then we performed this experiment again on another day and compared these values to the expected values.

	Number of atoms in gaseous state (Trial 1)	Number of atoms in gaseous state (Trial 2)
Temperature ^{o}C	n	n
25	1.21E+10	N/A
30	2.37E+10	3.48E+10
40	5.22E+10	6.06E+10
50	1.52E+11	1.22E+11
60	3.11E+11	2.68E+11
70	8.55E+11	7.05E+11
80	2.06E+12	1.46E+12
90	3.33E+12	2.75E+12
100	5.81E+12	N/A

Table 1

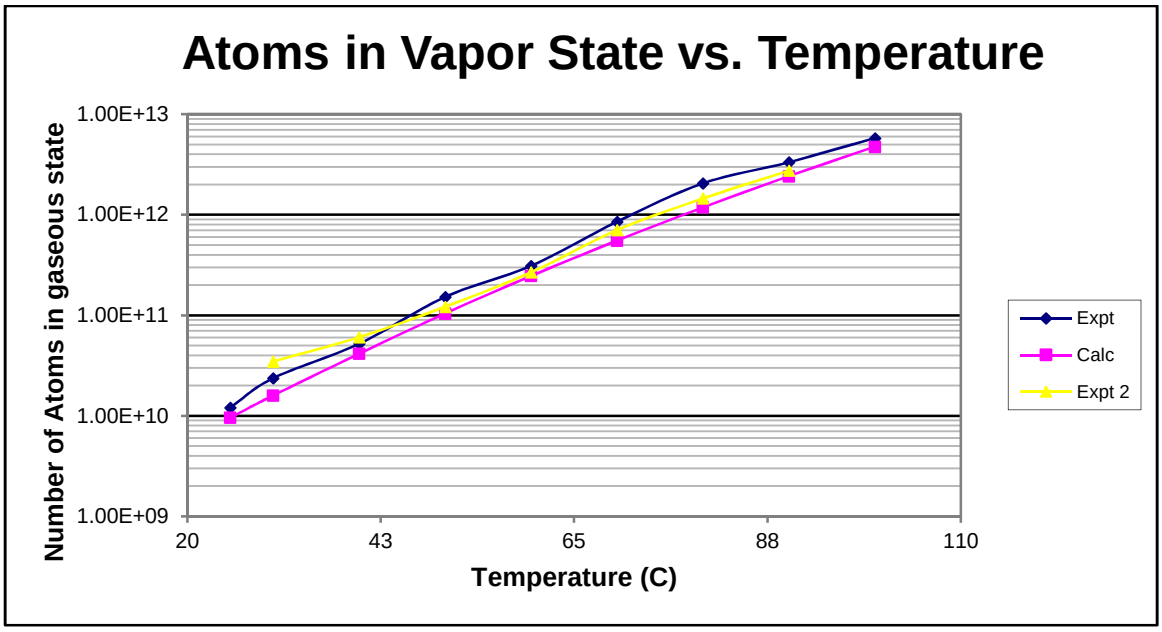

Figure 11: a graph detailing the expected value of atomic density compared to the experimental values.

Both of these measurements gave results that were very close to the expected values as shown in the Figure 11. The discrepancies observed in this graph most likely occurred for two different reasons. Firstly, outside light could have had a slight impact upon the measured value creating a difference. Secondly, the presence of Rubidium 85 in addition to the Rubidium 87 could have had an effect

upon how many atoms of rubidium are in a gaseous state. We accounted for the presence of rubidium but the exact percentage of each could have been off causing a difference in our calculated and our measured values.

4.2 EIT measurements of the Rubidium Atoms

The next part of the experiment focused upon the measurement of the strength of the magnetic fields through the use of EIT measurements. In order to do this we measured the frequency separation between various EIT resonances of the Rubidium atoms through a variety of light polarizations in order to determine the strength as well as the direction of the magnetic field. These results would then be compared to the previously measured magnetic field in order to see if there is an agreement between our measured values and our calculations.

The calculation of the magnetic field required the use of formula (1). For our experimental values we calculated the Δf to be equal to .45MHz and the u_B*g =(.7MHz/G) therefore plugging this into the formula is equal to

$$\frac{.45MHz}{m * \frac{.7MHz}{G}} = .651G$$

Which is very close to the previously measured value if totaling the overall magnetic field, which was equivalent to .6521G.

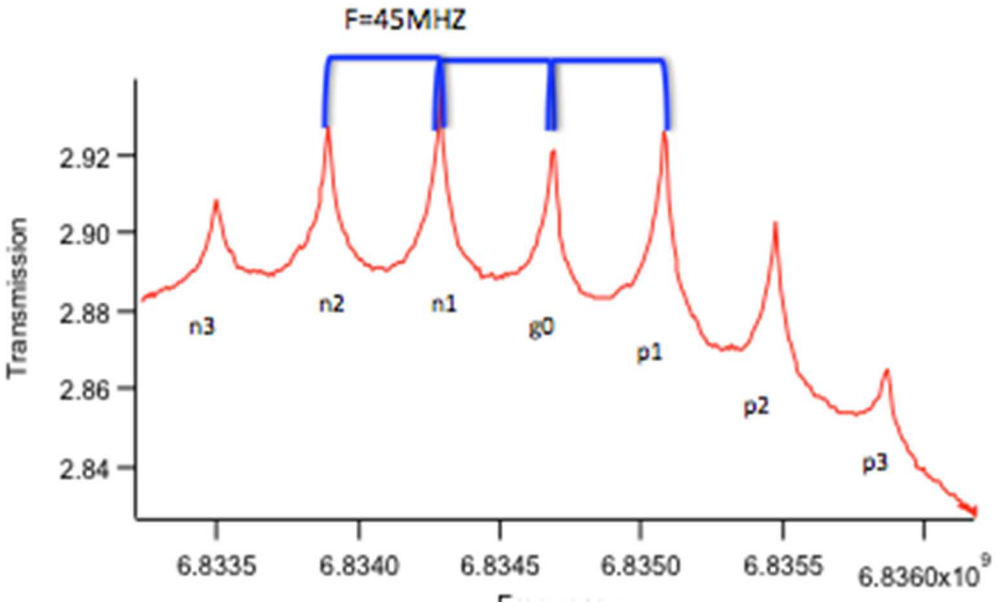

Figure 12: Graph showing the frequency change with voltage and the measured difference in frequency.

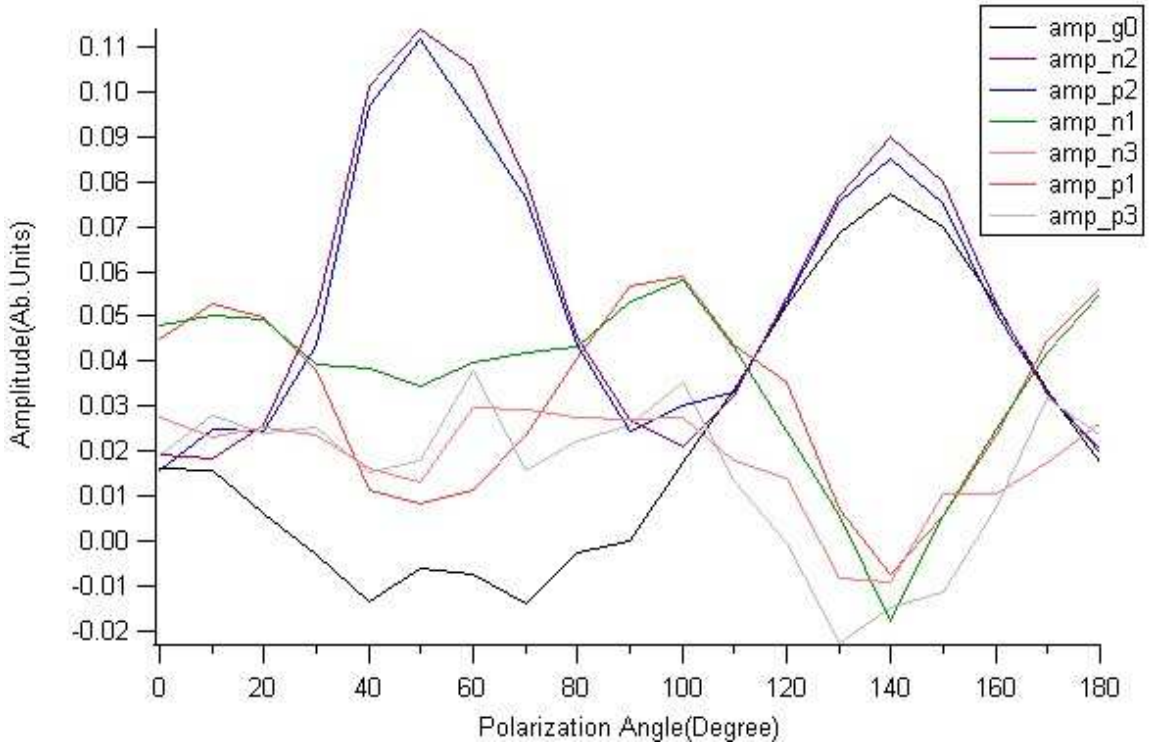

Figure 13: The measured Zeeman Sideband amplitude graph where different states refer to different peaks written in Figure 12

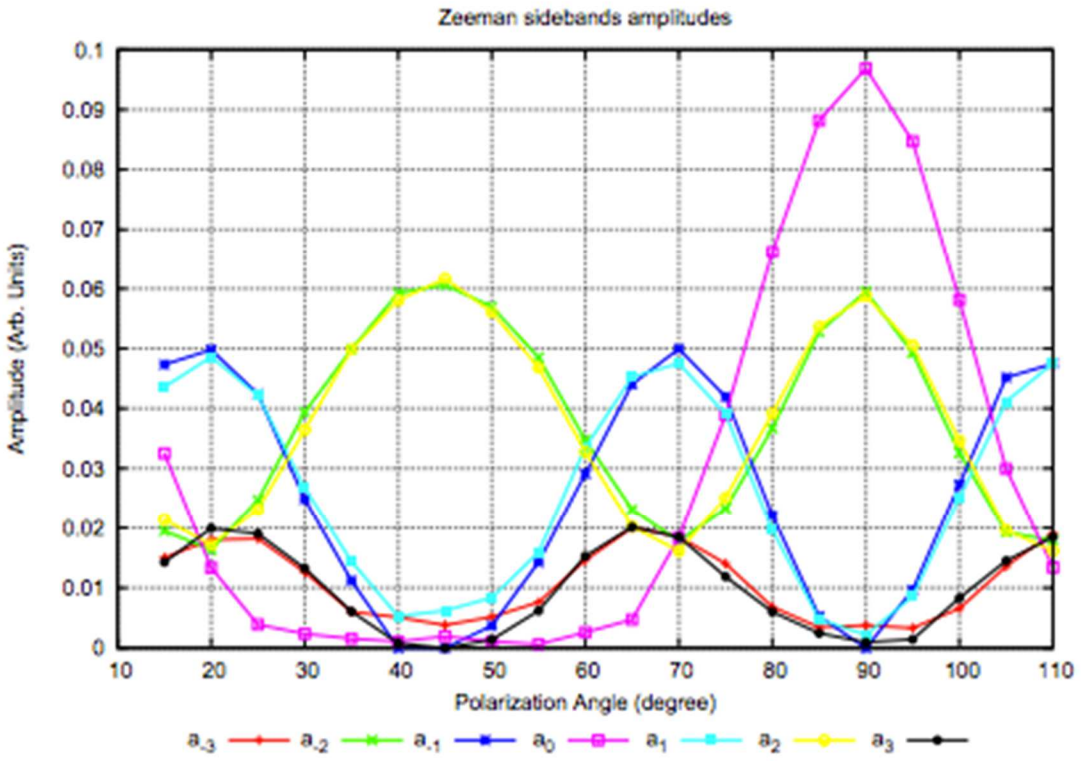

Figure 14: the experimental calculation for the Zeeman Sideband angles [4]

To find this polarization angle we then had to consult with previous experimental results on determining the polarization angle through the use of EIT measurements. To do this we measured the amplitude of the transmission peaks at differing polarizations. We then compared our experimental values to the theoretical values in order to determine the magnetic field direction.[4] Our values were close to the 0 degree measurements recorded in the report which was very similar to the actual measured angle of around 5 degrees implying that our calculated values with this new magnetometer were very close to our trial magnetometer.

4.3 Optimization of Magnetometer

Then we attempted to optimize this magnetometer to enable it to have sharp short peaks on the EIT readings. To do this we measured the slope of the derivative of the lines, the width of the peaks and the amplitude of the peaks. We did this for various circumstances ranging from the changing of the wave plate

orientation to the inclusion of a lens into the experimental setup to better focus the beam through the rubidium cell.

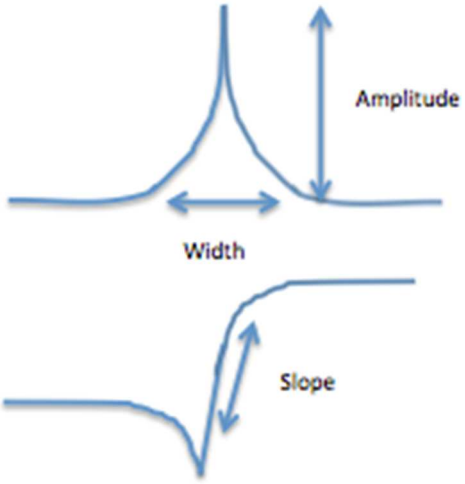

Figure 15: What width, amplitude and slope correspond to for the measurement of transmission peaks.

For the addition of a lens we ran the tests, which are recorded in figures 16, 17, and 18. As the results were actually becoming more unstable and there was little to no stability in the EIT measurements we concluded that not using a primary lens would be the best decision as there was very little difference any of the possible ways to increase the accuracy of the results.

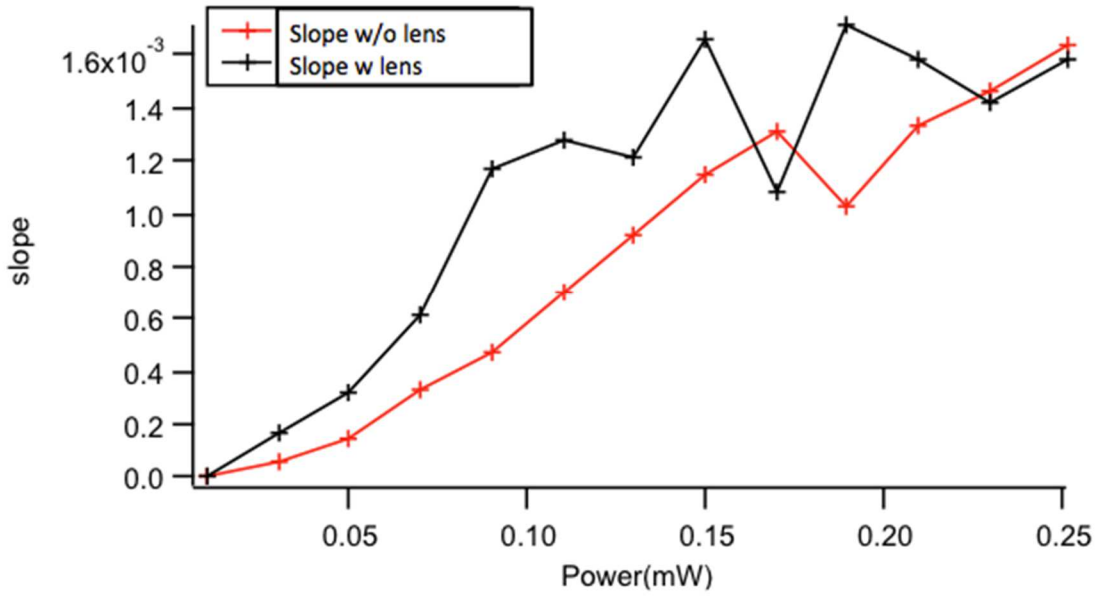

Figure 16: Graph of the Slope vs. Laser power

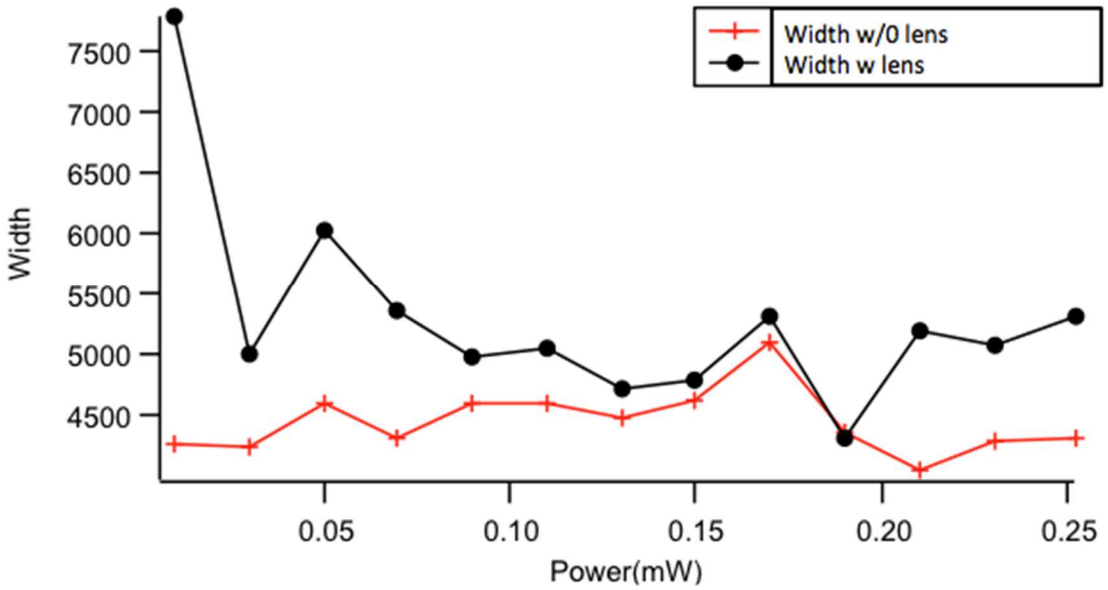

Figure 17: Graph of the Width vs. Laser power

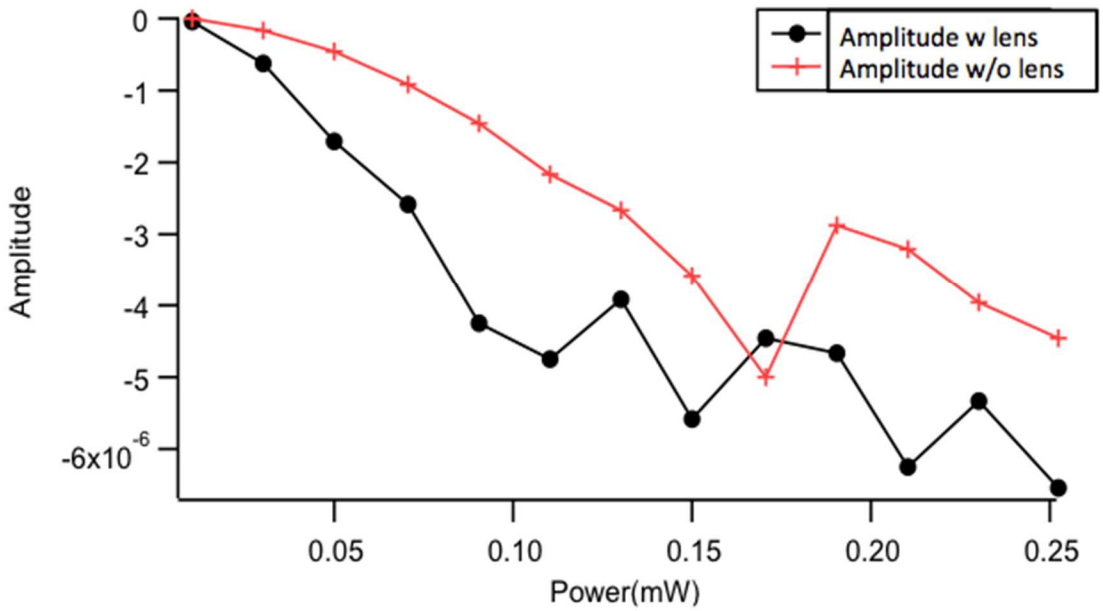

Figure 18: Graph of the Amplitude vs. Laser power where

For the measurements of the how the laser power effected the EIT measurements we varied the wave plate before the polarizer in order to get a clear view of the trend of the line when the polarizer was at 82 degrees. We then

recorded and graphed these measurements in order to identify at what power would the optimal measurements occur. The graphs for this are displayed in graphs 19, 20, and 21 below.

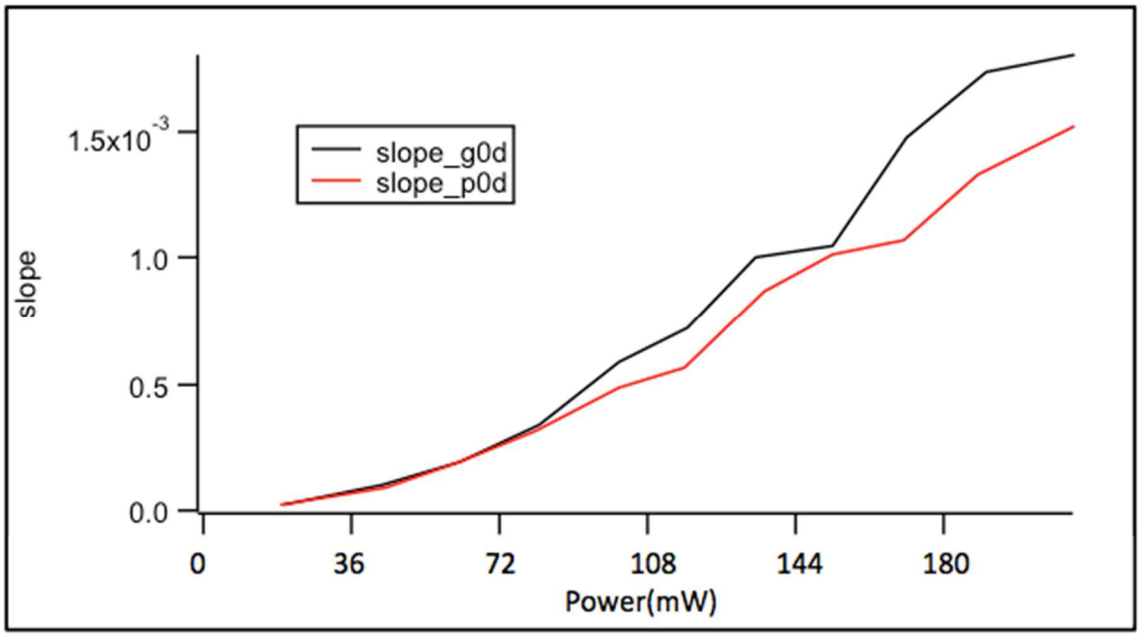

Figure 19: Slope vs. Laser power graph where g0 is the ground state and p0 is the first excited state

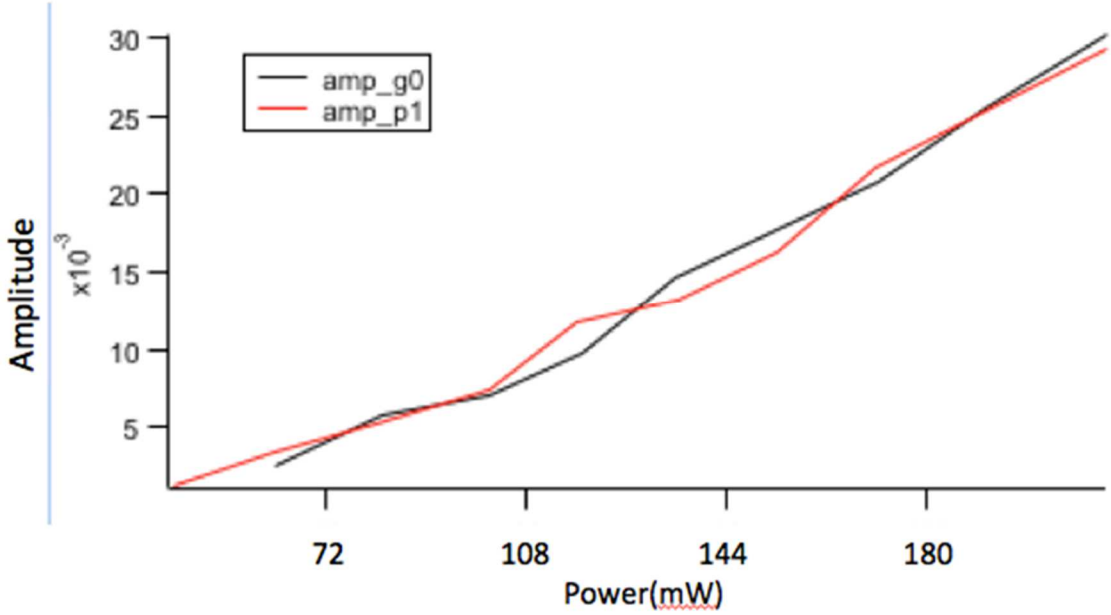

Figure 20: Amplitude vs. Laser power graph where g0 is the ground state and p0 is the first excited state

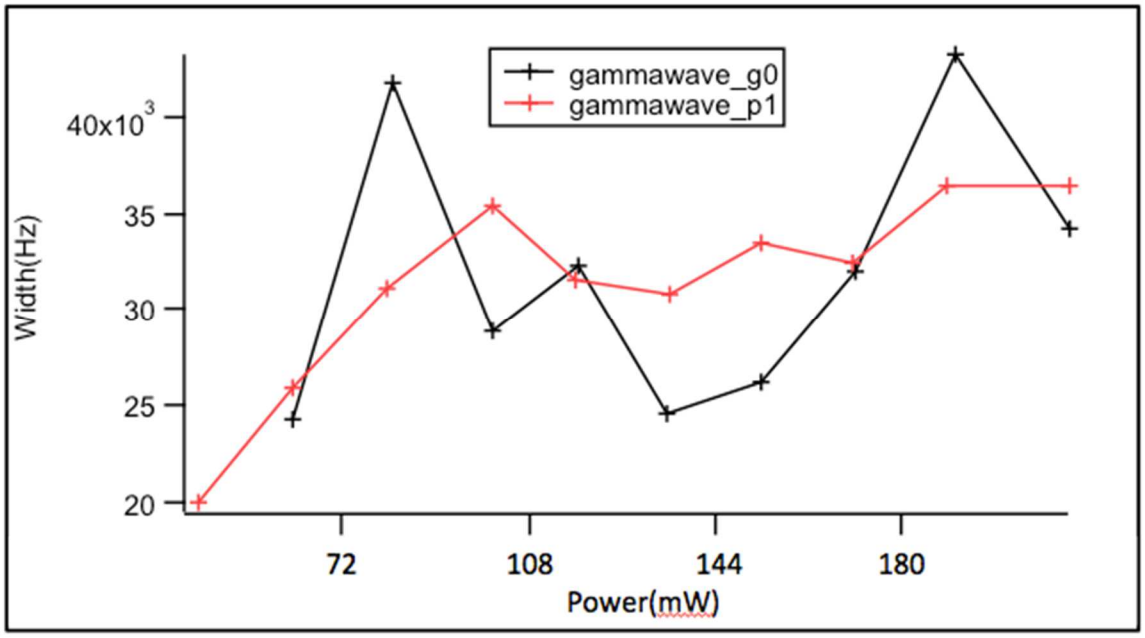

Figure 21: Width vs. Laser power graph where g0 is the ground state and p0 is the first excited state

We also conducted a comparison between magnetic-field-insensitive EIT peak (g0) and magnetic field sensitive EIT peak (p1). As detailed in both graphs the change in the polarization of 82 degrees allowed all of the points to be clearly expressed and for the p1 point to be of the same height in amplitude and slope as the ground state point. The changing of the wave plate did not have a huge affect upon the slope and the amplitude as when both of those values increased they were tied very closely together. However, in order to get these smooth derivatives we were attempting to minimize the gamma wave value, which was used to characterize the width of the waves. Using these graphs we could confirm that the ideal alignment would be when the current was between 70-100(mA) as in this range the width is at its minimum and the amplitude and slope are both very clearly defined.

4.4 Atomic Clock

The final phase of this project was focused on how well this experiment could function as an atomic clock. In order to do that we had to have a very stable measurement for the magnetic field and as such we were attempting to use the

previous information on the ideal situational setup to measure this.[5] In these measurements we provided a feedback to the microwave source, controlling the EIT resonance frequency to keep it locked to the peak of the EIT resonance. Through our previous data we aligned the magnetometer and had it function as a clock however, our magnetometer was not quite stable enough in order to function as a clock as over time the frequency the magnetometer would lose its lock and drift away. This would normally take approximately 45 minutes at the clock state area and about 10 minutes for the first positive magnetic resonance as recorded below. As such until the experiment undergoes more fine-tuning and optimizes this setup we cannot use the magnetometer for these purposes.

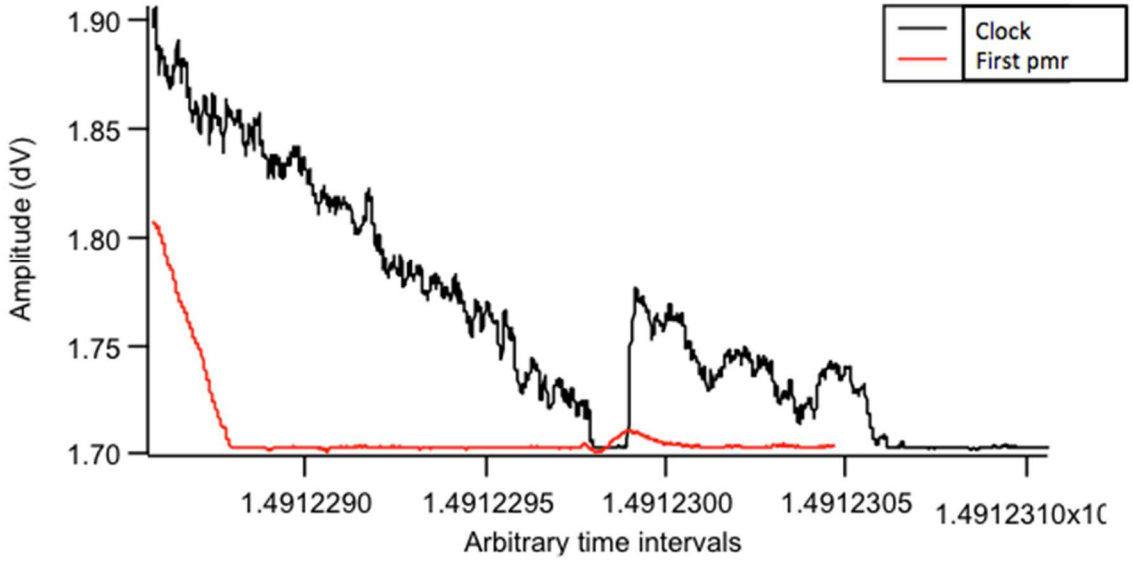

Figure 22: Amplitude vs. Time, where pmr represents positive magnetic resonance

In spite of this we did uncover just how good our magnetometer was at picking up magnetic fields as the reason behind most of the magnetic fluctuations that removed this magnetic lock was the temperature controlling unit fluctuating to allow current to flow into the heater. This was only a small electric current yet it was able to influence the magnetometer from approximately 1 meter away. This sensitivity showcases that this magnetometer could in fact function as an atomic clock in the future. As shown in Figure 23 this small change is clearly visible and

varies by approximately .03 depending upon the state of the temperature controller.

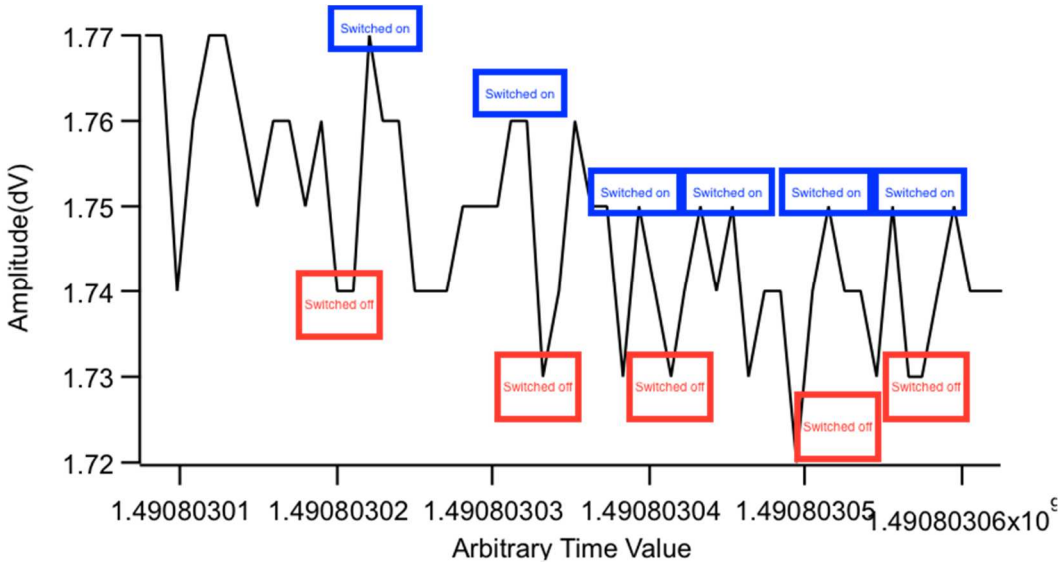

Figure 23: Amplitude vs. Time graph zoomed in on the first positive magnetic resonance

5. Conclusion

The main outcome of my project was the construction of a shield-free atomic magnetometer prototype. In this experiment we have concluded that there is a relatively stable magnetic field around the area of the apparatus, of approximately .651 G, so the magnetic field will not cause the distortion of the magnetometers readings. Also we have determined that the rubidium cell's experimental values for the number of atoms undergoing atomic transitions are approximately the number of atoms calculated to be undergoing this change. We then measured the magnetic field and direction through the EIT and determined that the values expected in our previous measurements were the same indicating that the casing-free magnetometer is functioning correctly. Then we also started calibrating the magnetometer to determine the ideal settings for the measurement of the magnitude and direction of the magnetic field. Moving on in the future I hope that this experiment can be used in he atomic clock setup more fully and display how much the EIT of this magnetometer fluctuates.

6. Refrences

[1]E. E. Mikhailov, I. Novikova, M. D. Havey, and F. A. Narducci,“Magnetic field imaging with atomic Rb vapor”, Optics Letters, Issue 22, 34, 3529-3531, (2009). Opt. Lett. 34, 3529 (2009).

[2]Ripka, P. (2001). *Magnetic sensors and magnetometers*. Boston: Artech House.

[3]D. J. Griffiths, Introduction to Quantum Mechanics, 2nd ed. Pearson Prentice Hall, Upper Saddle River, NJ, (2005).

[4]K. Cox, V. I. Yudin, A. V. Taichenachev, I. Novikova, and E. E. Mikhailov, “Measurements of the magnetic field vector using multiple electromagnetically induced transparency resonances in Rb vapor,” Phys. Rev. A 83, 015801 (2011).

[5]N. Belcher, E. E. Mikhailov, and I. Novikova,“Atomic clocks and coherent population trapping: Experiments for undergraduate laboratories”, Am. J. Phys. 77, 988 (2009).

[6]Secer, G., & Barshan, B. (2016). Improvements in deterministic error modeling and calibration of inertial sensors and magnetometers. Sensors and Actuators A: Physical, 247, 522-538.

[7]Ding, Z., Yuan, J., Wang, Z., Lu, G., & Luo, H. (1997, April 29). Optically pumped rubidium atomic magnetometer with elliptically polarized light. Optik - International Journal for Light and Electron Optics,127(13), 5270-5273.

[8]Chen, M., Yuan, J., Wang, Z., & Long, X. (2015). A compact super sensitive nonplanar ring laser magnetometer. Optik - International Journal for Light and Electron Optics, 126(2), 176-178.

7. Acknowledgment

I’d like to thank Irina Novikova for all of her guidance on this project. I would also like to thank Eugeniy Mikhailov for his help with some of the soldering of components and general help. Lastly, I would also like to thank my family and friends for encouraging me throughout the years.

.